Online ISSN: 2981-0396 Print ISSN: 2981-0388
International Journal of Iron & Steel Society of Iran
Journal Homepage: https://journal.issiran.com/

Research Article

Magnetic and Structural Properties of $SrFe_{12}O_{19}$ Nanoparticles Synthesized by Co-precipitation- Ultrasonic Method for Iron and Steel Industry Applications

T. Isfahani *[1], Z. Golshirazi [2]

Materials Engineering Group, Golpayegan College of Engineering, Isfahan University of Technology, Golpayegan, Iran

ARTICLE INFO

Keywords:

$SrFe_{12}O_{19}$, Co-Precipitation Method, Ultrasonic, Magnetic, Structural Properties.

Article history:

Received 11 October 2025
Received in revised form 13 November 2025
Accepted 09 May 2026

ABSTRACT

In the modern iron and steel industry, the application of advanced and improved systems is a necessity. One of the materials that has a great role in this improvement is strontium hexaferrite oxide. In this research, pure strontium hexaferrite oxide ($SrFe_{12}O_{19}$) particles were synthesized using the chemical co-precipitation method. The synthesis was done with and without applying ultrasonic radiation (UT). The Rietveld refinement was applied to the X-ray diffraction patterns of the synthesized $SrFe_{12}O_{19}$ powders. The Rietveld refinement indicated the successful synthesis of a single-phase M-type hexagonal $SrFe_{12}O_{19}$ phase. SEM analysis results showed that when the ultrasonic radiation is applied, the particle and crystallite sizes vary. The obtained particles had an agglomerated semi-spherical morphology. Synthesized particles obtained without the application of UT (SFO) had a mean particle size of 108.53±52nm. Application of UT radiation (UT-SFO) resulted in the reduction of the particle sizes to a mean value of 55.44±18.4nm. Magnetic properties showed that the saturation magnetization (Ms), remanent magnetization (Mr), and coercivity field (Hc) were 55.04, 29.54, and 2713.06 for the SFO sample. Values for the UT-SFO sample are 47.09, 25.53, and 2750.14, respectively. The results indicated that the synthesized samples have a Mr/Ms of around 0.54 and are suitable for magnetic applications and can be used in the iron and steel industry.

1. Introduction

Even though, strontium hexaferrite is not used in the primary iron and steel making process, and it is not a direct product of the steel industry, its properties make it essential in the steel industry. In other words, the connection between strontium hexaferrite and the iron and steel industry is multifaceted, depending on its composition and manufacturing process. Material handling systems, lifting magnets, and Eddy current separators, continuous casting machines (mold oscillators and electromagnetic stirrers (EMS)), motors, and generators are some of its applications. The use of strontium hexaferrite oxide enables technology to be used and convert the steel industry to a modern steel industry. For example, the strontium hexaferrite is used as a magnet. These strontium hexaferrite oxide magnets can be used in different sections to provide specific goals. Magnetic separators are also another main application. Lifting magnets, which are massive electromagnets, usually have the core or baseplate of strontium hexaferrite. The strontium hexaferrite provides a stronger magnetic

* *Corresponding Author*
Email: t.isfahani@yahoo.com
Address: Materials Engineering Group, Golpayegan College of Engineering, Isfahan University of Technology, Golpayegan, Iran
1. Associate Professor, 2. M.Sc.

DOI: http://10.22034/IJISSI.2026.2074328.1336
Published by ISSI (Iron & Steel Society of Iran)

field and provides a safety latch effect, which holds the scrap metal when the powder fails. Another application of strontium hexaferrite is raw material purification. In this case, the magnetic iron ore is separated from the non-magnetic gangue (waste rock). Scrap metal recycling in the steel industry is done by giant drums or overhead magnets made of strontium hexaferrite. These magnets are used to move, separate iron-based (ferrous) scraps from non-ferrous ones (such as trash, copper, aluminum, etc.). Also, the strontium hexaferrite can be used as a coolant filtration to remove unwanted iron particles present in the cooling and lubricating fluids, protects the machinery, maintains the product quality, and makes steel production efficient and cost-effective.

The Philips' laboratory introduced the M-type strontium hexaferrite ($SrFe_{12}O_{19}$) phase in 1950 [1, 2]. Chemically stable $SrFe_{12}O_{19}$ has a low cost and shows good magnetic properties. The good magnetic properties of $SrFe_{12}O_{19}$ gained the researchers' and scientists' attention. The low price of $SrFe_{12}O_{19}$ was due to the absence of rare earth elements in its compound [3-5]. $SrFe_{12}O_{19}$ with high coercivity is classified as a hard magnet and can be used as a permanent magnet. $SrFe_{12}O_{19}$ also has several applications and can be used in microwave devices, recording media, magneto-optical, and telecommunication devices [6-11], magnetic sensors, nanocomposites used for electromagnetic shielding, hyperthermia treatment, drug delivery systems, and the iron and steel industry [12-17].

The structure of M-type hexagonal consists of alternative stacks of spinel ($S=Fe_6O_8^{2+}$) and hexagonal ($R=MFe_6O_{11}^{2-}$) layers (Fig. 1.). O^{2-} ions in the close-packed layers are substituted by the M^{2+} ions in the hexagonal layer. Fe^{3+} ions are distributed in five interstitial crystallographic sites of the close-packed layers. These sites are the octahedral (2a, 12k, and $4f_2$), tetrahedral ($4f_1$), and trigonal bipyramidal (2b) sites. The ferrimagnetic structure of $SrFe_{12}O_{19}$ is formed by three parallel sites of 2a, 12k, and 2b and antiparallel sub-lattices of $4f_1$, and $4f_2$ sites, which are coupled with O^{2-} ions by the super exchange interactions [18-20]. It is well known that the synthesis conditions, particle size, particle shape, size distribution, and also the composition significantly affect the properties of ferrites [21-25]. It has been reported that the incorporation of ultrasonic vibration during the synthesis process is a powerful strategy to enhance and control the magnetic properties of nanoparticles synthesized by methods such as co-precipitation. The presence of ultrasonic vibration during the synthesis could lead to smaller, more crystalline, and less agglomerated particles[26-29].

So far, different methods have been applied to synthesize $SrFe_{12}O_{19}$ particles. Most used methods for the synthesis of $SrFe_{12}O_{19}$ are the co-precipitation[30], solid state [31], self-propagating high temperature synthesis [32], sol-gel process[33], and salt-melting methods[34]. It is well known that the magnetic properties of $SrFe_{12}O_{19}$ are affected by the shape and size of its synthesized particles [31, 35].

The co-precipitation method is a well-known, simple, and low-cost chemical method used for the synthesis of oxides. Zi et. al.[1] introduced a modified chemical co-precipitation method for synthesizing pure $SrFe_{12}O_{19}$ particles with regular hexagonal-shaped platelets in the range of 2 to 4μm. Davoodi et. al.[36] synthesized $SrFe_{12}O_{19}$ by the co-precipitation method in the presence of polyvinyl alcohol (PVA). They showed that the presence of PVA results in the reduction of calcination temperature, particle size, and coercivity. Palomino et. al.[37] sonochemically synthesized $SrFe_{12}O_{19}$ nanoparticles using a complexed polyol solution of metallic acetates and diethylene glycol. They focused on the effects of the sonication time and thermal energy on the crystal structure and magnetic properties. According to their results, first, an amorphous phase of Fe^{3+}, Fe^{2+}, and Sr^{2+} ions was obtained. Then this amorphous phase transforms to maghemite (γ-Fe_2O_3) and α-Fe_2O_3 at 300°C and 500°C, respectively. Finally, a rounded $SrFe_{12}O_{19}$ nanoparticle phase is formed at 800°C with an average particle size of 60 nm, magnetization of 62.3 emu/g, and coercivity of 6.25 kOe.

In this research, the co-precipitation method is used to synthesize single-phase $SrFe_{12}O_{19}$ powder with and without the application of ultrasonic radiation. The main focus is to use low-cost material, a simple process, and to avoid using additional material such as PVP, PVA, etc., which can limit its applications and negatively affect the properties. Also, the effect of using UT radiation on the phase formation, morphology, particle size, and particle size distribution is compared with the state of not applying UT. Moreover, the application of ultrasonic radiation on the structural and magnetic properties is discussed.

2. Experimental

In this research, pure single-phase $SrFe_{12}O_{19}$ powder was synthesized using the co-precipitation method with and without the application of UT. The synthesis process is schematically presented in Fig. 2. $Fe(NO_3)_3 \cdot 9H_2O$ and $Sr(NO_3)_2$ were used as the Fe and Sr sources, respectively. Strontium nitrate solution and iron nitrate solutions were prepared separately to provide a molar ratio of 1:12. (2.29 g $Fe(NO_3)_3 \cdot 9H_2O$ and 0.1g $Sr(NO_3)_2$). Each of the solutions was stirred using a magnetic stirrer to obtain a clear solution. The solutions were mixed. The mixed solution was magnetically and continuously mixed as presented in Fig. 2. (with and without the application of ultrasonic radiation) at 70°C for 1 hour until a clear solution was obtained. To get a pH of 13, 55 mL of 1M NaOH solution was added dropwise to the mixed solution. Resultant precipitates were centrifuged, dried at 100°C for 12 hours in an oven, sintered at 1000°C

(heating rate = 10°/min) for 2 hours in air (along with furnace cooling) using an alumina crucible, and finally ground. The centrifugation was done three times with water washing. The centrifugation was done using 10/000rpm for 15 minutes.

The obtained powders were characterized using a Philips XRD machine with CuKα_1 radiation. X-ray diffraction patterns were collected with a 2Θ range of 10-75°. Phase(s) and crystallite sizes of the powders were obtained by applying the Rietveld refinement to the XRD patterns. Topas software was used for the Rietveld refinement. Morphology and particle sizes were obtained using a Philips scanning electron microscope. ImageJ software was used to obtain the mean particle sizes. The mean particle size was obtained using three different images. Magnetic properties were measured at room temperature using a vibration sample magnetometer (VSM). The ultrasonic treatment was done using a KND-1200UH1 machine with a frequency of 19.5 kHz and 900-watt power. The cycle was a 60-second pulse and a 10-second rest. The probe was inserted at the center and the middle of the solution at room temperature.

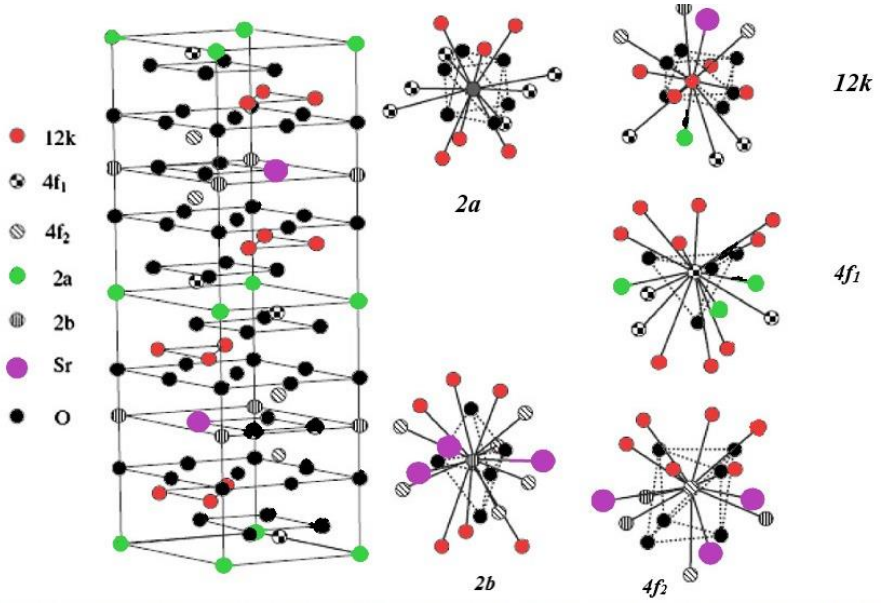

Fig. 1. The five Fe sites present in the hexagonal M-type $SrFe_{12}O_{19}$ crystal structure[38].

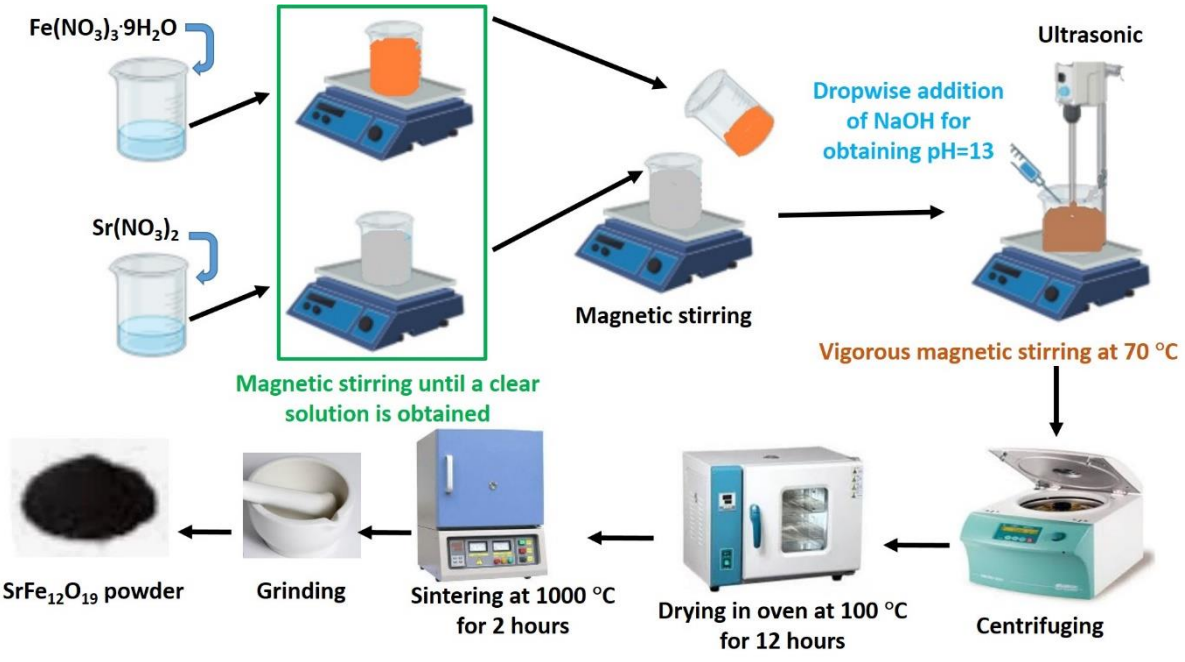

Fig. 2. The synthesis procedure used for obtaining $SrFe_{12}O_{19}$ particles with the application of ultrasonic radiation.

3. Results and Discussion

3.1. XRD Analysis

The Rietveld refinement was applied to the XRD patterns of the obtained $SrFe_{12}O_{19}$ powders (SFO and UT-SFO) as presented in Fig. 3. Results indicated that pure single-phase $SrFe_{12}O_{19}$ was synthesized without any undesired phases or impurities. The obtained structure of the synthesized $SrFe_{12}O_{19}$ is hexagonal magnetoplumbite, whereas $P6_3/mmc$ is the space group. Intensity and ratio of the XRD peaks are different in the two samples, indicating that they have different crystallite sizes. Rietveld refinement results show that the calculated crystallite size is 78.9nm and 44.7nm for the SFO and UT-SFO samples, respectively. Results indicate that with the application of UT radiation, the crystallite size decreases. It is also well known that the relative intensity of the diffraction peaks is related to the crystal structure, structure factor, and ionic scattering. The differences in the relative intensity in the diffraction phases are due to the preferred orientation obtained from the synthesis methods and conditions [39, 40]. In this study, the reduction in the XRD peak intensity observed for the sample prepared using UT radiation can also probably be attributed to the defect density within the crystalline structure and increased strain [40-42].

3.2. SEM Analysis

The SEM images of the SFO and UT-SFO samples are presented in Fig. 4(a) and 4(b). As can be observed, the particles have semi-spherical morphology, and the mean size is 108.53 and 55.44nm for the SFO and UT-SFO samples, respectively. Fig. 4(b). reveals that the application of UT does not have much effect on the morphology but significantly affects the size of the synthesized powders. The mean particle size of the UT-SFO is about half the mean particle size of the SFO sample. The particle size distributions are also presented in Fig. 4(c) and 4(d). The mean particle sizes and standard deviations are 108.53±52.17nm and 55.44±18.4nm for the SFO and UT-SFO samples, respectively. As presented, both samples have a wide particle size distribution, while the SFO sample has a broader particle size distribution. It should be noted that most of the particles do not have a hexagonal shape. Although, in both samples, as indicated in Fig. 4(a) and (b)., it can be seen that some of the particles have a morphology similar to a hexagonal shape. It is expected that the morphology of the particles converts into a plate-like polyhedral shape with the increase in the heat treatment temperature/ heat treatment time. The inhomogeneous and uneven particle sizes are due to the rapid and rigorous mixing during the synthesis procedure by magnetic stirring. The application of UT (UT-SFO sample) also results in more heterogeneity and particle size reduction. It has been reported [43] that ultrasonic vibration does not change the thermodynamic driving force (ΔG) but drastically modifies the kinetic pathways by which a system reaches equilibrium, leading to faster nucleation rates, a higher number of nuclei, and often a suppression of crystal growth, resulting in finer microstructures. Fig. 4. reveals that the particles are agglomerated. The existence of agglomerated particles is also probably due to the magnetic interactions present between the particles[44].

3.3. Magnetic Properties

The M-H loops of the SFO and UT-SFO samples obtained from the vibrating sample magnetometer (VSM) analysis are presented in Fig. 5. Magnetic properties are extracted from the M-H loops and presented in Table 1. The vibrating sample magnetometer studies showed that both of the pure $SrFe_{12}O_{19}$ synthesized samples have a typical semi-hard ferromagnetic behavior. The SFO sample has a coercive field of 2713.06 Oe and a remanent

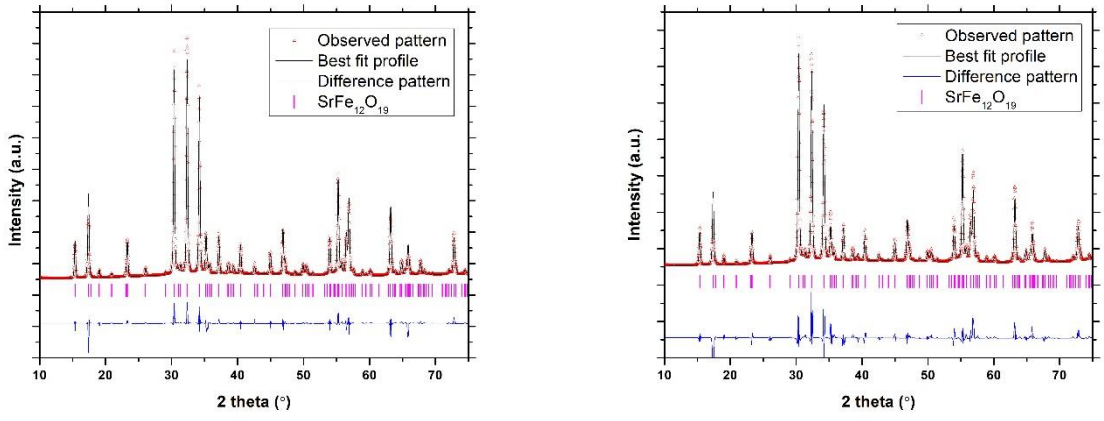

Fig. 3. The Rietveld refinement of the X-ray diffraction powders; (a) SFO (Rwp= 4.354, and GOF= 1.257) and (b) UT-SFO samples (Rwp= 6.812, and GOF= 1.948).

magnetization of 29.54 emu/g. In contrast, for the UT-SFO sample, the value of Hc is 2750.14, and the value of Mr is 25.53.

As mentioned earlier, the UT-SFO sample has a smaller mean particle and mean crystallite size, and as expected, the coercive field (Hc) has a higher value. The higher Hc value is consistent with the other published research. The Hc value significantly depends on the particle size/shape effect of the crystal anisotropy[45], and also the orientation of magnetic domains and microstructure. An increase in Hc indicates enhanced magnetic anisotropy and finer particles. Where, higher external magnetic fields are required for demagnetizing[46]. Moreover, higher coercivity can also be due to increased strain and defects in the particles. Increased strain and defects in the particles enhance the demagnetization resistance[46]. As mentioned, with the increase of Hc, the magnetic anisotropy enhances, and smaller particles are present. Smaller particles need higher external magnetic fields to demagnetize[47]. The utilization of UT in the synthesis procedure leads to higher coercivity. The utilization of UT is likely accompanied by increased strain and defects in the particles [48-52].

Moreover, the Ms value is also dependent on the particle size. Smaller particle sizes show lower values of Ms. It is well known that under an external field, the energy of the magnetic particles is proportional to the particle size [45]. In this research, the value of Ms for the SFO sample is 55.04, whereas it decreases to 47.09emu/g for the UT-SFO sample. Furthermore, the obtained saturation magnetization values in this research are not near the theoretical single-crystal strontium ferrite Ms value of 74.3emu/g [45]. The Ms value indicates that the powders are polycrystalline.

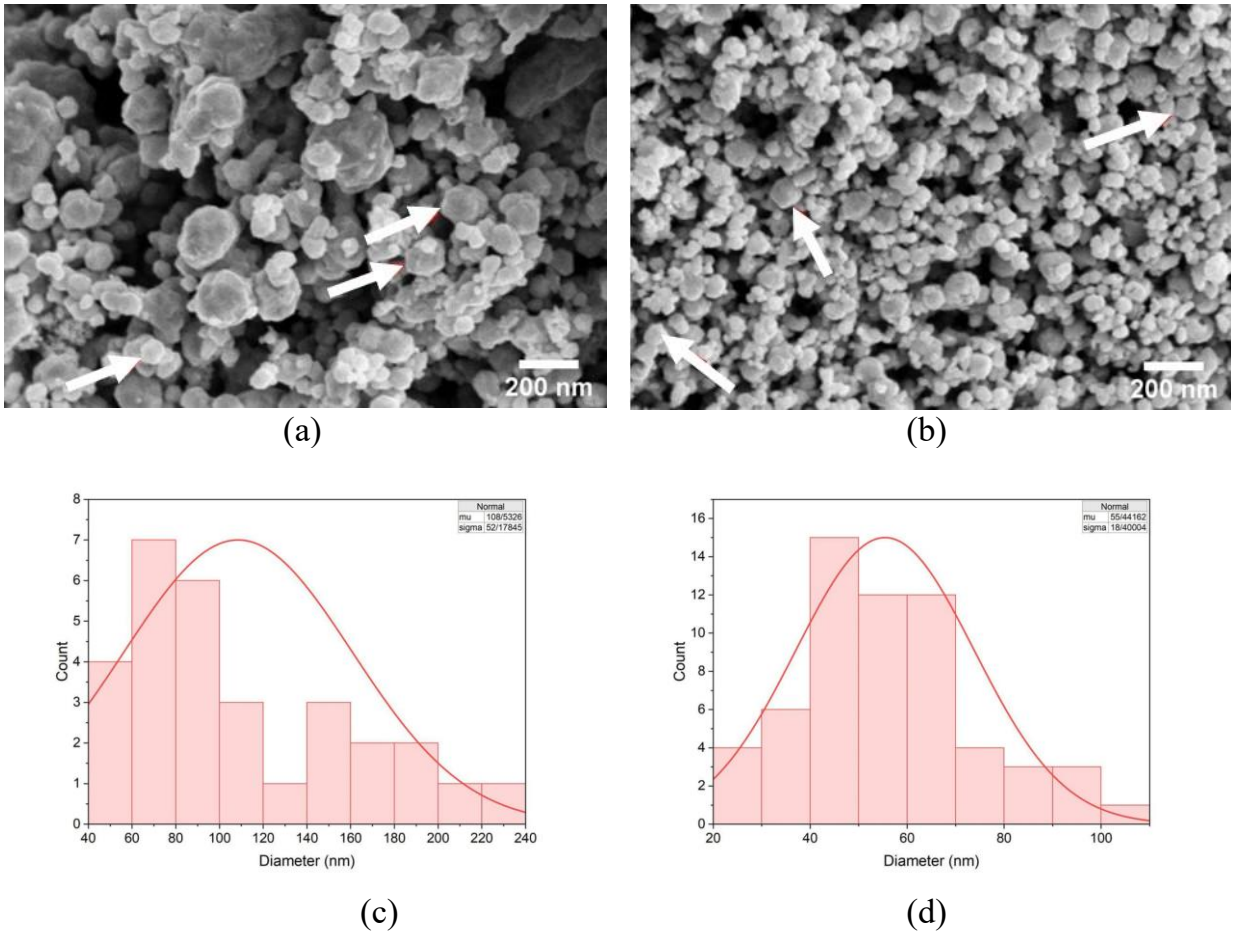

Fig. 4. The SEM image and particle size histogram of the SFO (a, c) and UT-SFO (b, d) samples.

Table 1. Magnetic parameters of the $SrFe_{12}O_{19}$ synthesized with and without the application of ultrasonic (SFO and UT-SFO samples).

Sample	Ms (emu g^{-1})	Mr (emu g^{-1})	Hc (Oe)	Mr/Ms
SFO	55.04	29.54	2713.06	0.537
UT-SFO	47.09	25.53	2750.14	0.542

The ratio of squareness (S) can be calculated by employing Eq.(1) as presented in Table 1.

$$S=Mr/Ms \qquad \text{Eq.(1)}$$

From the results presented in Table 1, it can be confirmed that the application of UT does not have a significant influence on the 'squareness ratio'. The S value is 0.537 and 0.542 for the SFO and UT-SFO samples, respectively.

The S value of 0.5 or near 0.5 indicates a material with intermediate or "semi-hard" magnetic properties, where the material retains only half of its saturation magnetization once the external field is removed. It should be mentioned that the magnetization reversal occurs primarily through the domain wall motion rather than the uniform rotation.

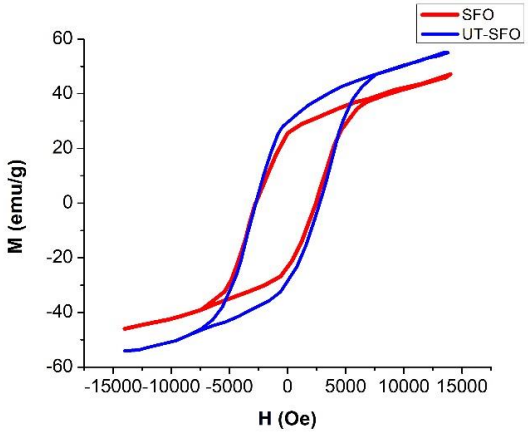

Fig. 5. The vibrating sample magnetometer (M-H loop) analysis of the samples obtained with and without the application of ultrasonic radiation.

As mentioned before, the magnetic properties strongly depend on the particle morphology[45]. Among the different particle morphologies, such as bubble, needle-like, rod-like, and spherical particles, the highest coercivity is shown to be for the needle-like particles. As a result, the magnetic properties can be tuned with the control of morphology, microstructure, particle size, and chemical composition. Control of morphology, microstructure, particle size, and chemical composition can be applied by using different synthesis methods such as co-precipitation, ball milling, sol-gel, etc.[45].

4. Conclusions

Strontium hexaferrite ($SrFe_{12}O_{19}$) was prepared using a co-precipitation- ultrasonic method, and the effect of applying ultrasonic radiation (UT) on the crystallite and particle size, morphology, and magnetic properties was investigated. The XRD and Rietveld analysis indicated the successful synthesis of pure single-phase $SrFe_{12}O_{19}$ (SFO) with a mean crystallite size of 78.9nm and 44.7nm for the SFO and UT-SFO samples, respectively. According to the SEM results, without the application of UT, the particles had a mean size of 108.53±52nm. Application of UT radiation (UT-SFO) resulted in the reduction of the particle sizes to a mean value of 55.44±18.4nm. Both samples had a semi-spherical morphology. The VSM results revealed the magnetic properties. The results indicated that the saturation magnetization (Ms), remanent magnetization (Mr), and coercivity field (Hc) were 55.04, 29.54, and 2713.06 for the SFO sample. Values for the UT-SFO sample are 47.09, 25.53, and 2750.14, respectively. The results indicated that the synthesized samples have a Mr/Ms around 0.54 and are suitable for magnetic applications and can be used in industries such as the iron and steel industry. Moreover, it was understood that the magnetic properties are significantly influenced by particle size. Generally, smaller particles lead to increased coercivity (Hc) and decreased saturation magnetization (Ms), while larger particles exhibit the opposite trend. While particle size is a major factor, other variables like the synthesis method, annealing temperature, and the presence of impurities or dopants can also influence the magnetic properties of $SrFe_{12}O_{19}$.

In summary, the magnetic properties of $SrFe_{12}O_{19}$ are highly tunable by controlling the particle size. By adjusting the synthesis and processing conditions, one can tailor the material's coercivity and saturation magnetization to suit specific applications such as material handling systems, lifting magnets, and Eddy current separators, continuous casting machines (mold oscillators and electromagnetic stirrers (EMS)), motors, and generators.

References

[1] Zi Z.F, et al. Structural and magnetic properties of $SrFe_{12}O_{19}$ hexaferrite synthesized by a modified chemical co-precipitation method, J Magn Magn Mater. 2008; 320(21): 2746-2751.

[2] Went J.J, et al. Hexagonal Iron-Oxide Compounds as Permanent-Magnet Materials, Phys Rev. 1952; 86(3): 424-425.

[3] Shirk B.T, Buessem W.R, Temperature Dependence of Ms and K1 of $BaFe_{12}O_{19}$ and $SrFe_{12}O_{19}$ Single Crystals, J Appl Phys. 1969; 40(3): 1294-1296.

[4] Rensen J.G, van Wieringen J.S, Anisotropic Mössbauer fraction and crystal structure of $BaFe_{12}O_{19}$, Solid State Commun. 1969; 7(16): 1139-1141.

[5] Kreber E, et al. Mössbauer measurements of the bipyramidal lattice site in $BaFe_{12}O_{19}$, J Phys Chem Solids. 1975; 36(4): 263-265.

[6] Kazin P.E, et al. Formation of submicron-sized $SrFe_{12}$−$xAlxO_{19}$ with very high coercivity, J Magn Magn Mater. 2008; 320(6): 1068-1072.

[7] Morisako A, et al. Properties of Ba-ferrite/AlN double-layered films for perpendicular magnetic recording media, J Magn Magn Mater. 2002; 242-245: 304-310.
[8] Hernández P, et al. Influence of sintering atmosphere on the magnetic after-effect in strontium ferrites, J Magn Magn Mater. 1996; 157-158: 123-124.
[9] Jin Z, et al. Magnetic properties of isotropic $SrFe_{12}O_{19}$ fine particles prepared by mechanical alloying, J Magn Magn Mater. 1998; 182(1): 231-237.
[10] Iqbal M.J, et al. Synthesis, physical, magnetic, and electrical properties of Al–Ga substituted co-precipitated nanocrystalline strontium hexaferrite, J Magn Magn Mater. 2008; 320(6): 881-886.
[11] Shirk B.T, Buessem W.R, Magnetic Properties of Barium Ferrite Formed by Crystallization of a Glass, J Am Ceram Soc. 1970; 53(4): 192-196.
[12] Stingaciu M, et al. Optimization of magnetic properties in fast consolidated $SrFe_{12}O_{19}$ nanocrystallites, RSC Adv. 2019; 9(23): 12968-12976.
[13] Giustini A.J, et al. Magnetic Nanoparticle Hyperthermia in Cancer Treatment, Nano Life. 2010; 01(01n02): 17-32.
[14] Koh I, Josephson L, Magnetic Nanoparticle Sensors, Sensors. 2009; 9(10): 8130-8145.
[15] Huangfu Y, et al. Fabrication and investigation on the PANI/MWCNT/thermally annealed graphene aerogel/epoxy electromagnetic interference shielding nanocomposites, Compos Part A Appl Sci Manuf. 2019; 121: 265-272.
[16] Wang L, et al. Electromagnetic interference shielding MWCNT-Fe_3O_4@Ag/epoxy nanocomposites with satisfactory thermal conductivity and high thermal stability. Carbon. 2019; 141: 506-514.
[17] Huangfu Y, et al. Fabrication and investigation on the Fe_3O_4/thermally annealed graphene aerogel/epoxy electromagnetic interference shielding nanocomposites, Compos Sci Technol. 2019; 169: 70-75.
[18] Lechevallier L, et al. Structural analysis of hydrothermally synthesized Sr1−xSmx$Fe_{12}O_{19}$ hexagonal ferrites, J Magn Magn Mater. 2004; 269(2): 192-196.
[19] Pieper M.W, Morel A, Kools F, NMR analysis of La+Co doped M-type ferrites, J Magn Magn Mater. 2002; 242-245: 1408-1410.
[20] Morel A, et al. Sublattice occupation in Sr1−xLaxFe_{12}−x$CoxO_{19}$ hexagonal ferrite analyzed by Mössbauer spectrometry and Raman spectroscopy, J Magn Magn Mater. 2002; 242-245: 1405-1407.
[21] Hlosta J, et al. Influence of calcination temperature and particle size distribution on the physical properties of $SrFe_{12}O_{19}$ and $BaFe_{12}O_{19}$ hexaferrite powders, Sci Rep. 2024; 14(1): 17564.
[22] Dippong T, et al. Investigation on the formation, structural, and photocatalytic properties of mixed Mn-Zn ferrites nanoparticles embedded in SiO_2 matrix, J Anal Appl Pyrolysis. 2021; 158: 105281.
[23] Dippong T, et al. Influence of Mn^{2+} substitution with Co^{2+} on structural, morphological, and coloristic properties of $MnFe_2O_4$/SiO_2 nanocomposites, Mater Charact. 2021; 172: 110835.
[24] Dippong T, et al. Sol-Gel Synthesis, Structure, Morphology and Magnetic Properties of Ni0.6Mn0.4Fe_2O_4 Nanoparticles Embedded in SiO_2 Matrix, Nanomaterials. 2021; 11(12): 3455.
[25] Dippong T, et al. Structural, morphological and photocatalytic properties of Ni-Mn ferrites: Influence of the Ni:Mn ratio, J Alloys Compd. 2022; 913.
[26] Sosa M.C.V, et al. Evaluation of ultrasonic energy and temperature on the structural, morphological, and magnetic properties of Fe_3O_4 nanoparticles, Solid State Sci. 2025; 162: 107880.
[27] Peng Y, et al. Effect of reaction condition on microstructure and properties of (NiCuZn)Fe(2)O(4) nanoparticles synthesized via co-precipitation with ultrasonic irradiation, Ultrason Sonochem. 2021; 71: 105369.
[28] Kumar A, Gangawane K.M, Synthesis and effect on the surface morphology & magnetic properties of ferrimagnetic nanoparticles by different wet chemical synthesis methods, Powder Technol. 2022; 410: 117867.
[29] Hassanjani-Roshan A, et al. Investigating the Effect of Ultrasound Intensity on the Magnetic Properties of Magnetite Nanostructures Synthesized by Sonochemical Method, Int J Eng. 2023; 36(6): 1034-1039.
[30] Pankov V.V, et al. Fine hexaferrite particles for perpendicular recording prepared by the coprecipitation method in the presence of an inert component, J Magn Magn Mater. 1993; 120(1): 69-72.
[31] Chen D.H, Chen Y.Y, Synthesis of strontium ferrite nanoparticles by coprecipitation in the presence of polyacrylic acid, Mater Res Bull. 2002; 37(4): 801-810.
[32] Qiao L, et al. The magnetic properties of strontium hexaferrites with La–Cu substitution prepared by SHS method, J Magn Magn Mater. 2007; 318(1): 74-78.
[33] Ghasemi A, Morisako A, Structural and electromagnetic characteristics of substituted strontium hexaferrite nanoparticles, J Magn Magn Mater. 2008; 320(6): 1167-1172.
[34] Guo Z-B, et al. Preparation and magnetic properties of $SrFe_{12}O_{19}$ particles prepared by the salt-melt method, J Magn Magn Mater. 1997; 175(3): 333-336.
[35] Ataie A, Heshmati-Manesh S, Synthesis of ultra-fine particles of strontium hexaferrite by a modified co-precipitation method, J Eur Ceram Soc. 2001; 21(10): 1951-1955.
[36] Davoodi A, Hashemi B, Yousefi M.H, Synthesis of coprecipitated strontium hexaferrite nanoparticles in the presence of polyvinyl alcohol, J Magn Magn Mater. 2011; 323(23): 3054-3057.
[37] Palomino R.L, et al. Sonochemical assisted synthesis of $SrFe_{12}O_{19}$ nanoparticles, Ultrason Sonochem. 2016; 29: 470-475.

[38] Collomb A, et al. Crystal Structure and Cobalt Location in the W-Type Hexagonal Ferrite [Ba]Co_2-W, phys status solidi (a). 1986; 96(2): 385-395.
[39] Tenorio Gonzalez F.N, et al. Reducing the crystallite and particle size of $SrFe_{12}O_{19}$ with PVA by high energy ball milling, J Alloys Compd. 2019; 771: 464-470.
[40] Guerrero-Serrano A.L, et al. Magneto-Structural Characterization of Strontium Substituted Lead Hexaferrite, J Supercond Novel Magn. 2012; 25(4): 1223-1228.
[41] Mocherla P.S.V, et al. Correlation between milling-induced strain, microstructure, and magnetic properties in anisotropic $SrFe_{12}O_{19}$ powders, Ceram Int. 2022; 48(18): 26669-26677.
[42] Sánchez-De Jesús F, et al. Mechanosynthesis, crystal structure and magnetic characterization of M-type $SrFe_{12}O_{19}$, Ceram Int. 2014; 40(3): 4033-4038.
[43] Li Z, et al. An Overview of Synthesis and Structural Regulation of Magnetic Nanomaterials Prepared by Chemical Coprecipitation, Metals. 2023; 13(1): 152.
[44] Kareem M.M, Influence of Calcination Temperature on Structural, Morphological and Magnetic Properties of M-Type Strontium Hexaferrite Powder Prepared by Sol-Gel Auto Combustion Route, J Nanostruct. 2025; 15(2): 431-445.
[45] Kumar N, et al. Impact of Particle Size on Room Temperature Ferrimagnetism of $SrFe_{12}O_{19}$, J Supercond Novel Magn. 2010; 23(4): 423-427.
[46] Omari L.H, et al. Effect of low amount Mn doping on structural and magnetic properties of $SrFe_{12}O_{19}$: Effective magnetic anisotropy study by Stoner - Wohlfarth model, Mater Today Commun. 2021; 27: 102257.
[47] Hou Y.H, et al. Effects of intrinsic defects and doping on $SrFe_{12}O_{19}$: A first-principles exploration of the structural, electronic and magnetic properties, J Magn Magn Mater. 2021; 538: 168257.
[48] Semaida A.M, et al. Correlation between Composition and Magnetic Properties of $SrFe_{12}O_{19}$/Co Nanocomposite Synthesized by the High Energy Ball-Milling Process, Key Eng Mater. 2022; 911: 77-85.
[49] İÇİN K, et al. Mechanochemical synthesis of $SrFe_{12}O_{19}$ from recycled mill scale: Effect of synthesis time on phase formation and magnetic properties, J Alloys Compd. 2021; 873: 159787.
[50] Eikeland A.Z, et al. Enhancement of magnetic properties through morphology control of $SrFe_{12}O_{19}$ nanocrystallites, Sci Rep. 2018; 8(1): 7325.
[51] Adam A.M, Elshafaie A, Ibrahim E.M.M, Structural and magnetic properties of Dy doped $SrFe_{12}O_{19}$ ferrites, Mater Today Commun. 2023; 35: 105884.
[52] Hölscher J, et al. Controlling structural and magnetic properties of $SrFe_{12}O_{19}$ nanoplatelets by synthesis route and calcination time, J Phys D Appl Phys. 2020; 53(47): 474002.